Materials Research Bulletin 48 (2013) 661–667

Contents lists available at SciVerse ScienceDirect

Materials Research Bulletin

journal homepage: www.elsevier.com/locate/matresbu

Synthesis and characterization of conducting polypyrrole/SBA-3 and polypyrrole/Na–AlSBA-3 composites

Marcos B. Gómez Costa, Juliana M. Juárez, María L. Martínez, Andrea R. Beltramone, Jorgelina Cussa, Oscar A. Anunziata *

Centro de Investigación en Nanociencia y Nanotecnología (NANOTEC), Facultad Regional Córdoba, Universidad Tecnológica Nacional, Maestro López y Cruz Roja Argentina, 5016 Córdoba, Argentina

ARTICLE INFO

Article history:
Received 3 May 2012
Received in revised form 21 September 2012
Accepted 6 November 2012
Available online 15 November 2012

Keywords:
A. Composites
A. Nanostructures
A. Polymers
C. Infrared spectroscopy
C. X-ray diffraction

ABSTRACT

Si-SBA-3 and Na–AlSBA-3 materials were synthesized for application in the preparation of composites. Silica mesoporous materials were obtained following the sol–gel method and post-synthesis alumination. Pyrrole-saturated hosts were prepared by adsorption of pyrrole into the mesoporous materials. The adsorption/desorption of pyrrole was studied by FTIR. Molecules of pyrrole would be adsorbed through aromatic ring to the host. The polymerization technique was performed by oxidative way using different oxidizing agents, ammonium persulfate and ferric chloride, after pyrrole adsorption on both hosts. TG, FTIR, BET, XRD, SEM and TEM were used to characterize the resulting composites. These studies show that polypyrrole is generated inside the channel of the hosts; conductivity studies show that the composites exhibit conductivities at room temperature and in the range of 1×10^{-7} and 1×10^{-6} S cm^{-1} depending on the host and the oxidizing agents.

1. Introduction

Mesoporous materials with a uniform mesopore structure and an extremely high specific surface area were extensively studied in the past decade [1,2] due to their potential application as catalysts, adsorbents for large organic molecules, and host/guest chemical supports. Typical mesoporous materials include amorphous or polycrystalline solids such as silica or transitional alumina, or modified layered materials such as pillared clays and silicates. A significant effort has been made to synthesize, within the mesoporous range, regular and well-defined pore structure materials [3–5]. In acidic media, pH ~ 2, the silicate species becomes cationic (I^+); however, cationic surfactant (S^+) can be used to synthesize mesoporous materials by the $S^+X^-I^+$ system. Here the counter ion X^- behaves as a shielding agent between S^+ and I^+. The materials synthesized through this procedure are known as "acid-prepared mesostructures" (APM) or SBA [6]. Due to different precipitation conditions and charge-balance requirements, acid-derived materials (SBAs) have thicker pore walls and a framework charge different from that of base-derived mesoporous materials.

Many studies [7–9] have proposed that the incorporation of metals (Al, Zn) via post-synthesis is a promising alternative method. Considering the lack of sodium aluminate stability (aluminum source) at low pH (like SBA-3 synthesis media), the procedure used for introducing aluminum was that of postsynthesis [10].

In recent years, conducting polymers have been the subject of particular interest to chemists and physicists. Polypyrrole (PPY), as a promising conducting polymer, has been widely studied because of its high polarizability, superior conductivity [11,12] and electrorheological properties [13–15]. It exhibits different properties in comparison with polyaniline and other conducting polymers. Therefore, the incorporation of PPY into the channels of mesoporous hosts may provide material with different electric characteristics.

There has been increasing interest in the development of mesoporous silica-supported nanocomposites due to their potential application in catalysis, as well as miniaturized electronic and optical devices [2,16,17]. Mesoporous silica materials display uniform pore structure and large surface area, which turns them into ideal hosts for the preparation of new nanostructured composite materials.

A number of studies have reported on the encapsulation of guest materials, such as semiconductors [18,19], metals [20,21] and polymer [22–26], into mesoporous silica hosts. The resultant nanocomposites exhibit unique properties which differ from those of bulk materials.

Meanwhile, there has been particular interest in materials where conducting polymer is confined in the channels of mesoporous host to produce novel structures, even at the

* Corresponding author. Tel.: +54 351 4690585.
E-mail address: oanunziata@scdt.frc.utn.edu.ar (O.A. Anunziata).

0025-5408/$ – see front matter © 2012 Elsevier Ltd. All rights reserved.
http://dx.doi.org/10.1016/j.materresbull.2012.11.030

molecular level. Encapsulation of conducting polymer can improve the mechanical, thermal and chemical stability of the assemblies, possibly allowing individual molecular wires to be addressed [27].

In this work, we report the first results of the development of adsorption/desorptions of pyrrole and their interaction with mesoporous materials. In addition, we report the advance in polypyrrole/SBA-3 and polypyrrole/Na–AlSBA-3 composites by two different methods, using different oxidants (ammonium persulfate and ferric chloride).

Thus, the objective of this work is to synthesize and characterize PPY/SBA-3 composites (nanowires of PPY inside the porous channels of nanostructured materials).

2. Experimental

2.1. Synthesis of SBA-3

The mesoporous aluminosilicate was synthesized employing the sol–gel method by hydrolysis of tetraethylorthosilicate (TEOS) at room temperature, in an aqueous acidic solution, using cetyltrimethylammonium bromide (CTAB) as surfactant. The procedure designed was the following: the surfactant was mixed with water and HCl; 3 g of TEOS were then added, stirring to form a mixture whose molar composition was: TEOS:H_2O:HCl:CTAB = 1:130:9.2:0.12 [10].

After 45 min, a white precipitate was obtained; then it was filtered, washed and dried at room temperature. The material was afterwards immersed in ethanol reflux for 6 h in order to extract the surfactant, and calcined at 823 K in air for 6 h. The material obtained was denoted as SBA-3.

2.2. Preparation of Na–AlSBA-3

The alumination procedure of SBA-3 was carried out as follows [10]: Silica SBA-3 (1 g) was stirred in 50 mL of water containing dissolved sodium-aluminate in different proportions, at room temperature for 20 h and pH of 5.6. The synthesis was carried out at this pH, because sodium aluminate is not stable in acid medium ($pH < 3$) and reacts rapidly with protons to generate aqueous Al^{3+} ions; if pH is higher, deposition of aluminum hydroxide will occur. The mixture was filtered, washed, dried at room temperature overnight and then calcined in air at 823 K for 5 h. Finally, Al-SBA-3 sample with theoretical Si/Al = 20 was obtained.

2.3. Pyrrole adsorption and in situ polymerization

SBA-3 and Na–AlSBA-3 samples, employed as hosts, were dehydrated at 673 K in a vacuum for 2 h at 2×10^{-3} mbar. Afterwards, it was exposed to equilibrium vapors from pyrrole during 24 h at 353 K to obtain pyrrole saturated hosts (PY-SBA-3 and PY-Na–AlSBA-3) according to the procedure described by Anunziata et al. [28–30]. In these conditions, the pyrrole/hosts saturation relation was reached. Self-supported wafers of PY-SBA-3 were used for FTIR studies, employing a vacuum cell with CaF_2 windows. The spectrum was first recorded in air and then in vacuum for 1 h at room temperature at 323, 373, 473, 573 and 673 K. The spectrum was recorded after cooling the sample in the vacuum cell at room temperature.

The oxidative polymerization of adsorbed polypyrrole (PPY) was carried out at 25 °C; 1 mL of ferric chloride ($FeCl_3$) 0.25 M (oxidant) was added to 50 mg of materials with pyrrole adsorbed, without stirring, and left at room temperature for 24 h. Finally, the materials were filtered, washed and dried at 323 K. The samples obtained were FePPY/SBA-3 and FePPY/Al-SBA-3 composites. The same procedure was carried out using ammonium persulfate ($(NH_4)_2S_2O_8$) as oxidant, obtaining the samples of SPPY/SBA-3 and SPPY/AlSBA-3 composites.

For comparison, bulk polypyrrole was synthesized following a typical synthesis at 0 °C and using ammonium persulfate as oxidant [31,32].

2.4. Characterization

The surface area was determined by the BET method with a Micromeritics Chemisorb 2720 apparatus, equipped with a TCD detector. A single-point surface area method was used and N_2 was employed as a physisorbed gas. The X-ray diffraction (XRD) patterns were recorded with a Philips X'Pert PRO PANalytical diffractometer under Cu Kα radiation (λ = 0.154 nm). Thermal studies (TGA) of the guest, hosts and composites were carried out with a thermal analysis instrument (TA Instruments 2950 TGA–DSC). The samples were exposed to a constant heating rate of 10 K/min from room temperature to 873 K, under nitrogen flow (10 mL/min). FTIR studies were performed in a JASCO 5300 Fourier transform infrared spectrometer (FTIR). KBr wafers were used to obtain the FTIR spectra for polypyrrole composites.

Scanning electron micrographs (SEM) were obtained by using a Nova NANOSEM 230 with EDS (FEI COMPANY). Samples were placed over an aluminum drum and covered with a gold film. The transmission electron microscopy (TEM) micrographs were taken on a TEM Philips EM 301 instrument, operated at 100 kV.

Direct current electrical conductivity measurements were performed using pellets improving the contacts with a silver layer. Powder composite samples were pressed into pellets of 6 mm diameter and 0.7 mm thickness in a press by maintaining 2 ton metric pressure. These pellets were subjected to conductivity measurements in a four-probe set-up, improving the contacts with a silver layer. Resistances were determined from the current-voltage behavior and converted into conductivity data using the dimensions of the pellet.

3. Results and discussion

3.1. Hosts characterization

The X-ray diffraction patterns of as made SBA-3 and AlSBA-3 materials are illustrated in Fig. 1a and b respectively, showing the reflection peaks in the low angle region, characteristic of mesostructures. The presence of three Bragg angles can be distinguished in hexagonal lattice symmetry, typical of SBA-3 structure. Moreover, XRD patterns indicate that the hexagonally ordered structure of SBA-3 was persistent after the modification procedure. A prominent peak, $h\,k\,l$ = [1 0 0] as well as weaker peaks of [1 1 0] and [2 0 0] were observed in XRD pattern of SBA-3, which allowed us to corroborate, that the obtained mesoporous sample has a highly ordered pore system with a high porosity. XRD parameters and BET results are shown in Table 1.

3.2. Pyrrole adsorption studies

The FTIR spectrum of pure pyrrole in the range of 1800–1300 cm^{-1} is shown in Fig. 2 and Table 2. We can see the bands assignments according to literature data. Lord and Miller [34] Publisher IR and Raman data in 1942, whereas more precise spectrum was reported by Navarro and Orza [35], employing gas-IR equipment.

Fig. 2 shows the original FTIR spectra for pure pyrrole and the adsorbed pyrrole at 353 K in vacuum over siliceous SBA-3 (PY-SBA-3) and Na–AlSBA-3 (PY-AlSBA-3) in 1800–1300 cm^{-1} range. Before the pyrrole adsorption, the host was heated at 673 K for 4 h in

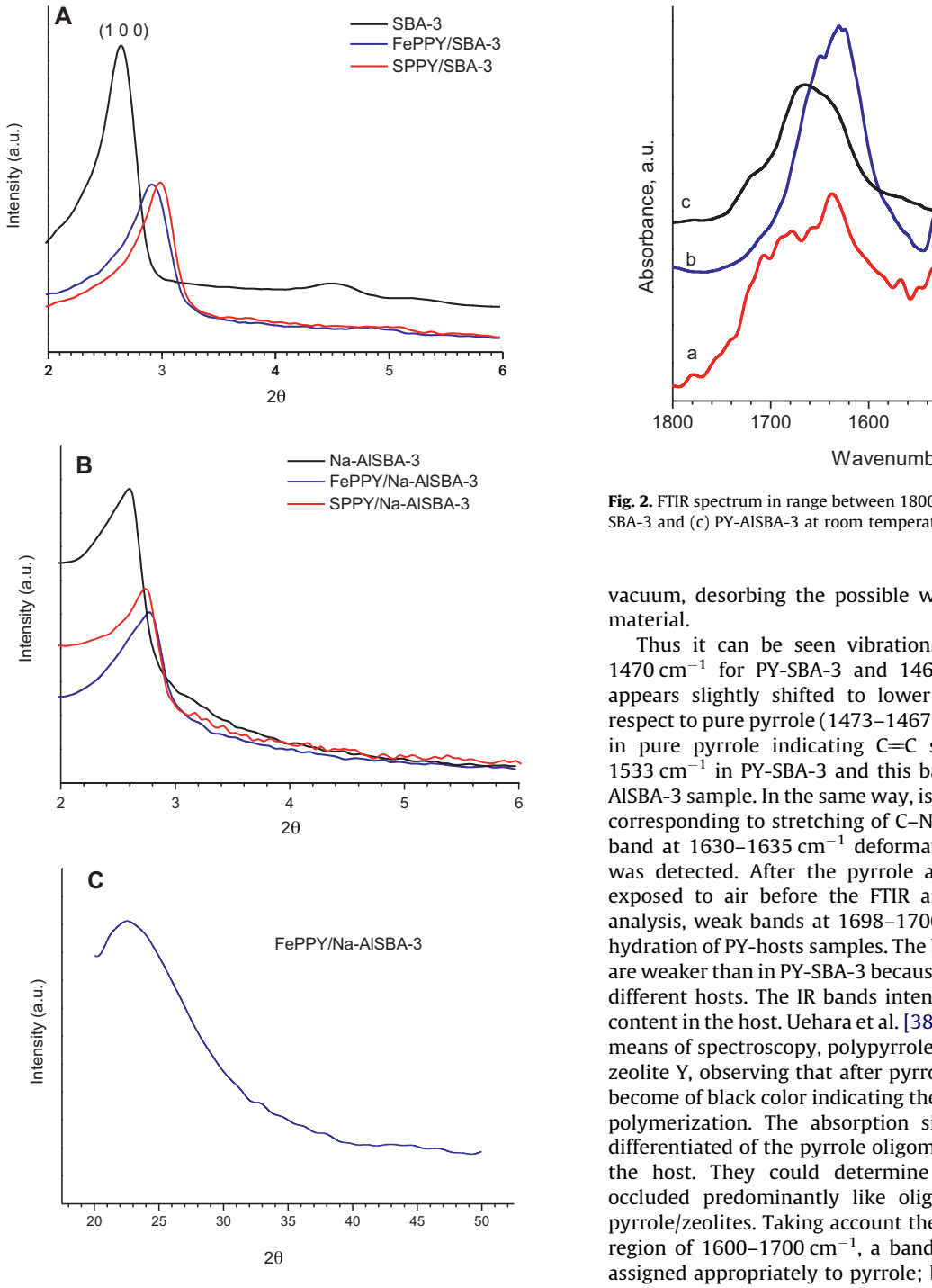

Fig. 1. X-ray diffraction patterns of the composites and the mesoporous materials used as hosts.

Fig. 2. FTIR spectrum in range between 1800 and 1300 cm^{-1} of (a) pyrrole, (b) PY-SBA-3 and (c) PY-AlSBA-3 at room temperature.

vacuum, desorbing the possible water molecules on the SBA-3 material.

Thus it can be seen vibrations of asymmetric C–N/C–C at 1470 cm^{-1} for PY-SBA-3 and 1460 for PY-AlSBA-3. This band appears slightly shifted to lower wavenumber in PY-AlSBA-3 respect to pure pyrrole (1473–1467 cm^{-1}). The band at 1527 cm^{-1} in pure pyrrole indicating C=C stretching vibration shifts to 1533 cm^{-1} in PY-SBA-3 and this band does not appeared in PY-AlSBA-3 sample. In the same way, is observed a band at 1420 cm^{-1} corresponding to stretching of C–N for both hosts. Additionally a band at 1630–1635 cm^{-1} deformation signal of water adsorbed was detected. After the pyrrole adsorption, the samples were exposed to air before the FTIR analysis. As the result of this analysis, weak bands at 1698–1706 cm^{-1} can be assigned to re-hydration of PY-hosts samples. The bands of pyrrole in PY-AlSBA-3 are weaker than in PY-SBA-3 because the amount of Py adsorbed in different hosts. The IR bands intensity increase with the pyrrole content in the host. Uehara et al. [38], studied and characterized by means of spectroscopy, polypyrrole formed in the channels of the zeolite Y, observing that after pyrrole was adsorbed, the samples become of black color indicating the occurrence of some oxidizing polymerization. The absorption signals of polypyrrole can be differentiated of the pyrrole oligomers and monomers existing in the host. They could determine that pyrrole molecules are occluded predominantly like oligomers and or monomers in pyrrole/zeolites. Taking account the previously exposed, in the IR region of 1600–1700 cm^{-1}, a band are observed that cannot be assigned appropriately to pyrrole; but the signal assigned to C–C vibration bonds between rings, was located at 1650 cm^{-1}. This signal is involved with a poor polymerization, carried out during the adsorption process. The signal at 1650 cm^{-1} was assigned to the C–C stretching between the rings of ter-pyrrole. The bands and

Table 1
Structural properties of the hosts.

Sample	Si/Al	XRD		A_{BET} (m^2/g)	Pore volume (mL/g)	Diameter pore[b] (nm)	Wall thickness[c](nm)
	Gel	d_{100}[a] (nm)	a_0[a] (nm)				
SBA-3	∞	3.13	3.6	1259	0.86	2.7	0.9
Al-SBA-3	20	2.95	3.4	810	0.50	2.46	0.94

[a] $d[h\,k\,l]$: interplanar spacing; a_0: lattice parameter ($a_0 = 2d[100]/\sqrt{3}$).
[b] $D \approx 4\,V/A$.
[c] $E = a_0 - D$ (according Ref. [33]).

Table 2
Pyrrole assignment bands according to literature data and IR absorption characteristics bands for PY-SBA-3 and PY-Na–AlSBA-3.

Bands assignments	Band position wavenumber (cm^{-1})		
	Pure pyrrole	PY-SBA-3	PY-Na–AlSBA-3
Re-hydration water	–	1707	1707
H_2O bending	–	1630	1630
Stretching C=C[a]	1521–1529	1533	–
Stretching C–C/C–N[b]	1473–1467 and 1422–1424	1470 and 1420	1460 and 1420
Bands assigned to oligomer compound (terpyrrole)[b]	–	1650	1650

[a] Ref. [36].
[b] Ref. [37].

their respective assignments can be observed in Table 2. Both hosts are capable to retain pyrrole for the in situ polymerization.

3.3. FTIR studies of polypyrrole/mesoporous materials

Fig. 3 shows FTIR spectra of pure polymer, silicate and aluminosilicate hosts and composites samples. The pure silica (Fig. 3A) and aluminated silica (Fig. 3B) show absorption bands at 1630, 1085, 964, 800 and 464 cm^{-1}. The peak at 1630 cm^{-1} is assigned to the OH bending vibrations of the water molecules adsorbed [39]. Typical asymmetric and symmetric Si–O–Si stretching vibrations are centered at 1085 and 800 cm^{-1}, respectively. The band at 969 cm^{-1} corresponds to Si–OH vibrations of the surface silanols, characteristic of mesoporous silica, but absent in the Na–AlSBA-3, which indicates that the surface silanol groups around 964 cm^{-1} interact with the Al species and contribute to form the Si–O–Al superficial species in the process of preparation of Na–AlSBA-3 [39].

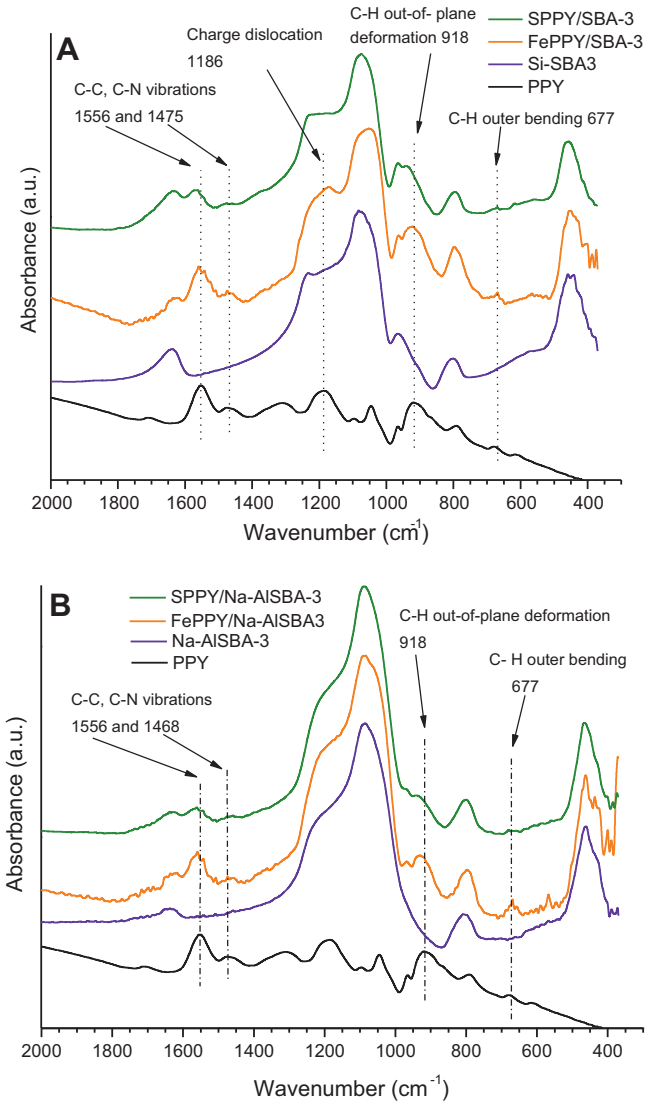

Fig. 3. FTIR spectra of (A) polypyrrole, SBA-3, and composites: FePPY/SBA-3 and SPPY/SBA-3; (B) polypyrrole, Na–AlSBA-3 and composite: FePPY/Na–AlSBA-3 and PPY/Na–AlSBA-3.

The synthesized polypyrrole (Fig. 3 and Table 3) shows bands at 1556 cm^{-1} (combination of intra-ring C=C and inter-ring C–C vibration), 1475 cm^{-1} (vibrations C–C, C–N), 1305 cm^{-1} (=C–N in-plane vibration), 1186 cm^{-1} (charge dislocation), 1045 cm^{-1} (C–N), 918 cm^{-1} (C–H out-of-plane deformation), 790 C–H cm^{-1} (out-of-plane bending), 677 cm^{-1} C–H (outer bending) and 613 cm^{-1} (C–H in-plane vibration) [40,41].

Sharp bands of PPY can be observed on the composites prepared (Fig. 3). Composites show sharp polypyrrole bands around 1560, 1475, 930 and 677 cm^{-1}, see Table 3. In the spectrum of FePPY/SBA-3 sample, a band at 1170 cm^{-1} (corresponding to charge dislocation band of pure PPY, 1186 cm^{-1}) can be seen overlapped with the Si–O–Si stretching band of the host. This can be attributed to the higher surface area of the SBA-3 than the aluminated sample, thus a good polymerization and a pyrrole adsorption higher than that in Al-SBA-3 were found in SBA-3.

The band at 1630 cm^{-1} corresponds to water bending, typical in mesoporous materials.

The samples do not show terpyrrole bands, which would have to be found at 1444 and 1414 cm^{-1}, indicating that the pyrrole is fully polymerized [36].

The bands of the composite corresponding to the polypyrrole also show a little shift to higher wavenumbers with respect to the pure polypyrrole. This indicates that the polymer chains are shorter in the composite compared with those of the pure compound. [41]. Instead, the spectra of the SPPY/SBA-3 and SPPY/Na–AlSBA-3 show bands at 1570 and 1560 cm^{-1}, shifted to a wavenumber higher than that of the corresponding of pure PPY (1556 cm^{-1}). In general, this peak tends to shift to a lower wavenumber as the conjugated length of polymer is increased. Therefore, the PPY chain in the composite is considered to be shorter than the length of pure PPY, and shorter than the samples polymerized with $FeCl_3$ [36,42]. The same bands showed in the spectrum of FePPY/SBA-3 and FePPY/AlSBA-3 composites are well defined than SPPY/SBA-3 and SPPY/AlSBA-3 samples.

The band at 1533 cm^{-1} that not appeared in Al-SBA-3, indicates that it's possible that the pyrrole rings are more perturbed because interaction between Na^+ cation or SiOH groups acid sites of Al-SBA-3.

3.4. X-ray diffraction studies

Fig. 1 shows the X-ray diffraction patterns of the SBA-3, the Na–AlSBA-3 and their corresponding composites.

Table 3
FTIR absorption characteristics bands of pure PPY and composites.

Assignment	Band position, wavenumber (cm^{-1})				
	Pure PPY	FePPY/SBA-3	SPPY/SBA-3	FePPY/AlSBA-3	SPPY/AlSBA-3
H_2O bending	–	1630	1630	1630	1630
Intra-ring C=C and inter-ring C–C	1556	1558	1570	1558	1560
C–C, C–N	1475	1475	1475	1475	1475
=C–N in-plane	1305	–	–	–	–
Charge dislocation	1186	1170	–	–	–
C–N	1045	–	–	–	–
C–H out-of-plane deformation	918	926	941	929	940
Out-of-plane bending	790	–	–	–	–
Outer bending	677	677	677	677	677
C–H in-plane	613	–	–	–	–

The SBA-3 shows a very intense diffraction [1 0 0] peak at 2.6° and two weaker peaks, [1 1 0] and [2 0 0], typical of the SBA-3 structure [43]. However, in the Na–AlSBA-3, only the [1 0 0] peak is easily distinguishable, since the change in the surface of the material is induced by the post alumination process [10].

In all the XRD patterns of the composites, a decrease in peak intensity and a subtle shift to higher 2θ can be observed with respect to the mesoporous materials alone (Fig. 1A and B). The decrease in intensity is commonly found in other mesoporous materials, with other guests confined in its interior, like polypyrrole/SBA-15 [41] and polyaniline/SBA-15 [44], and metal/mesoporous silica composites [45]. This can be ascribed to a relatively low scattering contrast between the pores and the walls of the mesoporous materials due to the formation of polypyrrole chains inside the meso channels [28,45]. In both methods the characteristic [1 0 0] peak of the SBA-3 remains after the polymerization process, suggesting that the structure persist. In the composites formed using SBA-3, the peaks [1 1 0] and [2 0 0] disappear after the formation of polypyrrole because of the polypyrrole inside the material, commonly found when polyaniline is incorporated inside of the MCM-41 channels, according to the reported by Feng et al. [46].

In these figures it can be noted that plane [1 0 0] in the composite, characteristic of SBA-3, shifts to higher 2θ angles. The shift in the diffraction plane indicates that the two components (polymer and host) have been successfully integrated and the structure of composite is more orderly and uniform than that in pure PPY [47]. At a higher angle (Fig. 1C), evidence of amorphous material can be seen, however, no polypyrrole peak is found because the polymer is inside the material pores.

3.5. Surface area, TEM and SEM analyses

The BET specific surface area decreases with the Al content, from 1259 m^2/g (SBA-3) to 810 m^2/g for AlSBA-3 Si/Al = 10, due to the loading of the pores by guest species, as well as to the major contribution of the additional mass Al_2O_3 in the sample [39].

Table 4 shows the area of the different composites. In all the composites, a decrease can be found in the specific area, indicating that polypyrrole could be within the channels of the corresponding SBA hosts.

Table 4
Surface area and conductivity of the hosts and composites.

Sample	Surface area (BET) (m^2/g)	Area % reduction	Conductivity ($S\,cm^{-1}$)
SBA-3	1259	–	–
FePPY/SBA-3	361	71.32	3.37×10^{-6}
SPPY/SBA-3	393	68.78	1.12×10^{-6}
Na–AlSBA-3	810	–	–
FePPY/Na–AlSBA-3	289	64.32	5.23×10^{-7}
SPPY/Na–AlSBA-3	315	61.11	1.28×10^{-7}

An ordered channels array could be observed from the TEM micrograph for SBA-3 sample (Fig. 4A), therefore mesoporous silica particle exhibits a well-ordered mesostructure and a typical honeycomb structure (cylindrical pores are viewed from the side as a stripped image).

To establish the morphology of the aluminated material, SEM studies reveal that the incorporation of aluminum (Fig. 4B) in the SBA-3 pores has no apparent effect on the macroscopic morphology of the samples. The SEM images of the samples show aggregates of regular spherulitic-shaped particles. The particle size of the AlSBA-3 is approximately 2–4 μm in diameter.

Fig. 4C shows SEM image of FePPY/SBA-3 sample. Virtually no difference in particle surface morphology was observed between the host and the composite material. Large clusters of pure PPY cannot be seen outside SBA-3 channels. The well regular shape and morphology are the same in all of composite samples.

3.6. Thermal analysis

Fig. 5 shows the TGA curve analysis for polypyrrole; the host Na–AlSBA-3, and the composites. For pure polypyrrole, the initial weight loss (300–373 K) is caused by the loss of water from the polymer. The polymer is thermally stable up to 430 K. From this temperature on, the polymer starts to degrade rapidly.

The Na–Al-SBA-3 shows a constant but slight weight loss with increasing temperature. The weight loss is about 4% around 373 K and then stabilizes with a total weight loss of 8.3% when reaching 873 K. The same behavior was found for Si-SBA-3 (not shown).

In all the composites, the initial weight loss below 373 K can be attributed to the loss of water and to some gases adsorbed from the composites.

It should be noted that for FePPY/Si-SBA-3 and SPPY/Si-SBA-3, the decomposition (evacuation) of encapsulated PPY is slower than that for pure polypyrrole. This slower decomposition of the encapsulated PPY implies diffusional constraints in the channels system [41]. If we considered the weight loss of pure PPY and guest PPY in the composite (FePPY/Si-SBA-3) at 620 K, a notable difference can be shown (30% and 18%, respectively); however, at 860 K this difference would be much wider (61.5% and 26.5%, respectively). Thus, this means that PPY becomes more stable as a guest in the host forming the composite, preventing the polymer from a fast degrading.

It is interesting to note that SBA-3-composites have more amount of PPY than AlSBA-3 composites. This fact can be seen in the difference in weight loss. At 860 K the difference of weight loss between FePPY/Si-SBA-3 and FePPY/Al-SBA-3 is approximately 12% (26% and 14%, respectively).

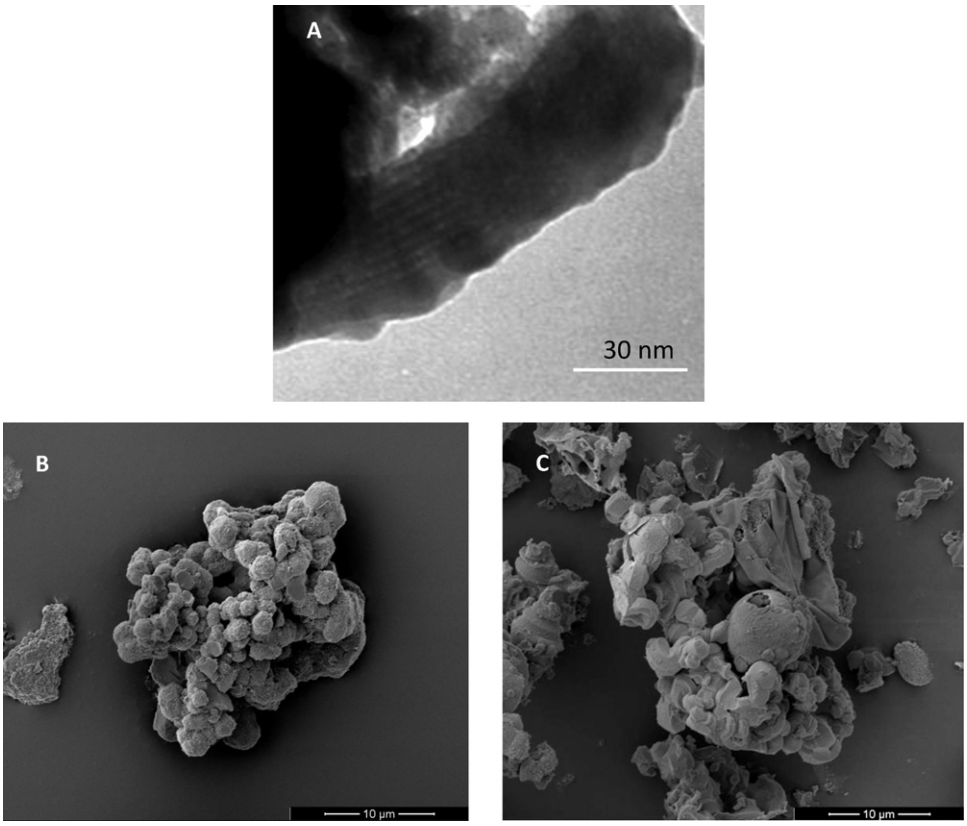

Fig. 4. (A) TEM image of SBA-3 and SEM images of (B) Na–Al-SBA-3 and (C) FePPY/SBA-3 composite.

3.7. Conductivity studies of composites

According to literature data the electrical conductivity for chemically synthesized polypyrrole is 10^{-2}–10^{-1} S cm^{-1} [44], and 10^{0} S cm^{-1} [41], polymerized with ammonium persulfate and ferric chloride respectively.

Table 4 shows the electrical conductivity of composites at room temperature. The composites have an electrical conductivity lower than that of pure polymer.

We can deduce that most PPY is located within the channels rather than on the surface of SBA-3 and AlSBA-3 mesoporous materials [41]. The mesoporous materials are highly insulating.

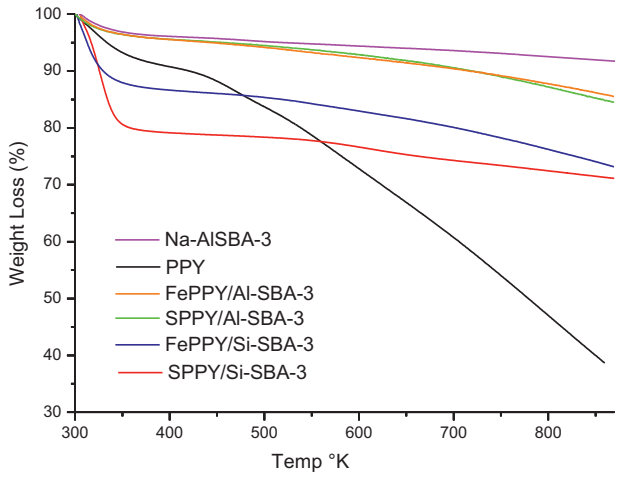

Fig. 5. TGA analysis for: pure polypyrrole, Na–Al-SBA-3 (host) and the different composites.

When PPY is inside the pores of meso or microporous aluminosilicates (SBA, MCM, zeolites, etc.), the conductivity of the composite can change from insulate to ionic conductors through semiconductors. The mechanism of conduction in polymers, e.g., polyfuran, polyindole, polypyrrole and polyaniline, is highly complex, since such materials exhibit conductivity in a range of about ten orders of magnitude by changing their doping. To explain the electronic phenomena in these systems, the concepts of solitons, polarons and bipolarons have been used [48,49]. Conduction in conducting polymers (enhancing or dipping) is influenced by numerous factors: polaron length, conjugation length, overall chain length and charge transfer to adjacent molecules [50]. Both conjugation length and redox potential are affected by their nature and substituent positions on the ring [51]. When the polymer is encapsulated in the host channels, conductivity may change. The mesoporous nanomaterial (SBA, MCM) used as a host affects the movement of the charges in the polymer. The results also show that the conductivity of the composite is lower than that of pure PPY.

SBA-3 based composites show better conductivity than that of Al-SBA-3 nanostructured composites, and composites obtained by polymerization with ferric chloride show higher conductivity than that of those polymerized with ammonium persulfate.

The synthesized composites have conductivities in order of 10^{-6}–10^{-7} S cm^{-1}, the composites synthesized with ferric chloride has a better conductivity than materials synthesized with ammonium persulfate. The conductivity of FePPY/SBA-3 is similar to composite PPY/SBA-15 [41], because the structure of silica SBA-15 is very similar to SBA-3; but the conductivity of SPPY/Na–AlSBA-3 composite is similar to composite PPY/MCM-41 [52].

The fact that FePPY/SBA-3 and SPPY/SBA-3 composites present conductivity higher than that of PPY/AlSBA-3 composites arises from the larger amount of conductive PPY described by the FTIR

analysis. According to the FTIR spectra, the conductivity of the samples is higher in the samples with sharper polypyrrole bands; thermogravimetric analysis shows a large amount of PPY in SBA-3-composites. Generally, it is assumed that conductivity should be higher in higher degrees of crystallinity and better alignment of the chains. The PPY included in FePPY/SBA-3 is more conducting and possibly more doped.

4. Conclusions

The nanoporous material Si-SBA-3 and mesoporous sodium aluminosilicate material Na–AlSBA-3 with longitudinal channel array were synthesized and characterized.

The technique of pyrrole adsorption was effective. The spectrum of PY-SBA-3 is more similar to pure pyrrole than FTIR spectrum of PY-AlSBA-3, indicating that more amount of pyrrole is adsorbed on SBA-3 host and both hosts are capable to retain pyrrole after the in situ polymerization.

The characterization of PPY-composites shows that it is possible to obtain pyrrole in situ polymerization within the Si-SBA-3 and Na–AlSBA-3.

The FePPY/SBA-3 composite shows a high degree of polymerization and a large amount of PPY.

The conductivity of the composites varies mainly according to hosts (SBA-3 or AlSBA-3) and according to the oxidizing agent.

The conductive behavior of composites would be modified by varying anchored sites of the host structure, the oxidizing agent, and the amount of PPY in the host. The potentially interesting and significant factor is that the polymer used to produce the composite structure inside the channels of SBA-3 can be altered according to the requirements of the final composite.

These composites offer numerous desirable properties with a high potential for successful application in the electronic field for developing, for example, an electronic device at nanometric scale. Organic molecular wires, together with inorganic reservoirs (SBA-3 and AlSBA-3), have thus been successfully developed into the channels, generating hybrid composites.

Acknowledgments

MBGC, MLM, ARB, JC and OAA CONICET Researchers; JMJ CONICET doctoral fellowship, are grateful to CONICET, Argentina, PIP No. 112-200801-00388 (2009–2013) and MinCyT-CBA PID: 1210/07 (2007–2012) y Proyecto GRF (2010–2012).

References

[1] C.T. Kresge, M.E. Leonowicz, W. Roth, J.C. Vartulli, J. Beck, Nature 359 (1992) 710–712.
[2] J.S. Beck, J.C. Vartuli, W.J. Roth, M.E. Leonowicz, C.T. Kresge, K.D. Schmitt, C.T.-W. Chu, D.H. Olson, E.W. Sheppard, S.B. McCullen, J.B. Higgins, J.L. Schlenker, J. Am. Chem. Soc. 114 (1992) 10834–10843.
[3] O.A. Anunziata, A. Beltramone, M.L. Martinez, L. López Belon, J. Colloid Interface Sci. 315 (2007) 184–190.
[4] F. Chen, H.-K. Luo, Y.-F. Han, C. Wang, G.J. Gan, Catal. Today 131 (2008) 76–81.
[5] A. Galarneau, D. D-Giscard, F. Di-Renzo, F. Fajula, Catal. Today 68 (2001) 191–200.
[6] G. Soler-Illia, C. Sanchez, B. Lebeau, J. Patarin, Chem. Rev. 102 (2002) 4093–4138.
[7] S. Zeng, J. Blanchard, M. Breysse, Y. Shi, X. Shu, H. Nie, D. Li, Microporous Mesoporous Mater. 85 (2005) 297–304.
[8] S. Kowalak, K. Stawinski, A. Mackowiak, Microporous Mesoporous Mater. 44 (2001) 283–293.
[9] T. Klimova, L. Lizama, J.C. Amezcua, P. Roquero, E. Terrés, J. Navarrete, J.M. Domínguez, Catal. Today 98 (2004) 141–150.
[10] O.A. Anunziata, M.L. Martínez, M.B. Gómez Costa, Mater. Lett. 64 (2010) 545–548.
[11] G. Tourillon, F. Garnier, J. Electroanal. Chem. 135 (1982) 173–178.
[12] Y. Lu, G. Shi, C. Li, Y. Liang, J. Appl. Polym. Sci. 70 (1998) 2169–2172.
[13] S.Z. Wu, F. Zeng, J.R. Shen, Polym. J. 30 (1998) 451–454.
[14] J.W. Kim, F. Liu, H.J. Choi, S.H. Hong, J. Joo, Polymer 44 (2003) 289–293.
[15] Y.D. Kim, I.C. Song, J. Mater. Sci. 37 (2002) 5051–5055.
[16] D. Zhao, J. Feng, Q. Huo, N. Melosh, G.H. Fredrickson, B.F. Chmelka, G.D. Stucky, Science 279 (1998) 548–552.
[17] L.M. Bronstein, S. Polarz, B. Smarsly, M. Antonietti, Adv. Mater. 1333 (2001) 13–17.
[18] X.G. Zhao, J.L. Shi, B. Hu, L.X. Zhang, Z.L. Hua, J. Mater. Chem. 13 (2003) 399–403.
[19] S.Z. Wang, D.G. Choi, S.M. Yang, Adv. Mater. 14 (2002) 1311–1314.
[20] A. Ghosh, C.R. Patra, P. Mukherjee, M. Sastry, R. Kumar, Microporous Mesoporous Mater. 58 (2003) 201–211.
[21] T. Asefa, R.B. Lennox, Chem. Mater. 17 (2005) 2481–2483.
[22] G.S. Attard, J.C. Glyde, C.G. Goltner, Nature 378 (1995) 366–368.
[23] S.W. Ho, T.K. Kwei, D. Vyprachticky, Y. Okamoto, Macromolecules 36 (2003) 6894–6897.
[24] D.J. Cardin, S.P. Constantine, A. Gilbert, A.K. Lay, M. Alvaro, M.S. Galletero, H. Garia, F. Marquez, J. Am. Chem. Soc. 123 (2001) 3141–3142.
[25] A.M. Showkat, K.P. Lee, A.I. Gopalan, M.S. Kim, S.H. Choi, H.D. Kang, Polymer 46 (2005) 1804–1812.
[26] P.L. Llewellyn, U. Ciesla, H. Decher, R. Stadler, F. Schuth, K.K. Unger, Stud. Surf. Sci. Catal. 84 (1994) 2013–2020.
[27] D.J. Cardin, Adv. Mater. 14 (2002) 553–563.
[28] M.L. Martínez, F.A. Luna D'Amicis, A.R. Beltramone, M.B. Gómez Costa, O.A. Anunziata, Mater. Res. Bull. 46 (2011) 1011–1021.
[29] O.A. Anunziata, M.B. Gómez Costa, M.L. Martínez, Catal. Today 133–135 (2008) 897–905.
[30] O.A. Anunziata, M.B. Gómez Costa, R.D. Sánchez, J. Colloid Interface Sci. 292 (2005) 509–516.
[31] N. Bloemberger, N. Laureate, Handbook of Advance Electronic and Photonic Materials and Device, Academic Press, San Diego, USA, 2001, p. 16.
[32] V. Shaktawat, N. Jain, M. Dixit, N.S. Saxena, K. Sharma, T.P. Sharma, Indian J. Pure Appl. Phys. 46 (2008) 427–430.
[33] F. Chen, A. Shen, X.-J. Xu, R. Xu, F. Kooli, Microporous Mesoporous Mater. 79 (2005) 85–91.
[34] R. Lord, F. Miller, J. Chem. Phys. 10 (1942) 328–341.
[35] R. Navarro, J. Orza, An. Quim. Ser. A 79 (1983) 557.
[36] S. Lamprakopoulos, D. Yfantis, A. Yfantis, D. Schmeisser, J. Anastassopoulou, T. Theophanides, Synth. Met. 144 (2004) 229–234.
[37] M. Kofranek, T. Kovář, A. Karpfen, H. Lischka, J. Chem. Phys. 96 (1992) 4464–4473.
[38] H. Uehara, M. Miyake, M. Matsuda, M. Sato, J. Mater. Chem. 8 (1998) 2133–2136.
[39] M.L. Martínez, M.B. Gómez Costa, G.A. Monti, O.A. Anunziata, Microporous Mesoporous Mater. 144 (2011) 183–190.
[40] M. Kofranek, T. Kovář, H. Lischka, A. Karpfen, J. Mol. Struct. – Theochem 259 (1992) 181–198.
[41] Q. Cheng, V. Pavlinek, A. Lengalova, C. Li, Y. He, P. Saha, Microporous Mesoporous Mater. 93 (1–3) (2006) 263–269.
[42] Y. Furukawa, S. Tazawa, Y. Fujii, I. Harada, Synth. Met. 24 (1988) 329–341.
[43] F. Chen, X. Xu, S. Shen, S. Kawi, K. Hidajat, Microporous Mesoporous Mater. 75 (2004) 231–235.
[44] X.T. Li, W.C. Geng, T. Zhang, Y. Zuo, S.L. Qiu, J. Appl. Polym. Sci. 93 (2004) 1597–1601.
[45] Y. Shana, L. Gao, Mater. Chem. Phys. 89 (2–3) (2005) 412–416.
[46] X. Feng, G. Yang, Y. Liu, W. Hou, J. Zhu, J. Appl. Polym. Sci. 101 (2006) 2088–2094.
[47] X. Sun, J. Ren, L. Zhang, L. Chen, H. Li, R. Li, J. Ma, Synth. Met. 160 (2010) 2244–2249.
[48] N.V. Blinova, J. Stejskal, M. Trchová, J. Prokes, Mária Omastová, Eur. Polym. J. 43 (2007) 2331–2341.
[49] A.J. Heeger, in: T.A. Skotheim (Ed.), Handbook of Conducting Polymers, vol. II, Dekker, New York, 1986, p. 729, and references therein.
[50] J.I. Kroschwitz, in: J.I. Kroschwitz (Ed.), Electrical and Electronic Properties of Polymers: A State-of-the-Art Compendium, Wiley, New York, 1988 , pp. 1–330.
[51] M. Leclerc, G. D'Aprano, G. Zotti, Synth. Met. 55 (1993) 1527–1532.
[52] Q. Cheng, V. Pavlinek, A. Lengalova, C. Li, T. Belza, P. Saha, Microporous Mesoporous Mater. 94 (2006) 193–199.